Available online at www.sciencedirect.com
ScienceDirect
Engineering Fracture Mechanics 75 (2008) 1171–1183
Engineering Fracture Mechanics
www.elsevier.com/locate/engfracmech

Multiple scattering of shear waves and dynamic stress from a circular cavity buried in a semi-infinite slab of functionally graded materials

Chao Hu [a,b], Xue-Qian Fang [b,*], Wen-Hu Huang [b]

[a] *School of Aerospace Engineering and Applied Mechanics, Tongji University, Shanghai 200092, China*
[b] *Department of Aerospace Engineering and Mechanics, Harbin Institute of Technology, P.O. Box 137, Harbin 150001, China*

Received 29 June 2006; received in revised form 15 January 2007; accepted 20 April 2007
Available online 16 May 2007

Abstract

Based on the theory of elastodynamics and employing image method, the multiple scattering and dynamic stress in a semi-infinite slab of functionally graded materials with a circular cavity are investigated. The analytical solution of this problem is derived, and the numerical solutions of the dynamic stress concentration factor around the cavity are also presented. The effects of the distance between the cavity and the boundaries of the semi-infinite slab, the incident wave number and the non-homogeneity parameter of materials on the dynamic stress concentration factors are analyzed. Analyses show that the dynamic stress around the cavity increases with increasing non-homogeneity parameter of materials and incident wave number. The boundaries of the semi-infinite slab have great effect on both the maximum dynamic stress and the distribution of dynamic stress around the circular cavity, and the effect increases with increasing incident wave number.

Keywords: Exponentially graded materials; Multiple scattering of elastic waves; Dynamic stress concentration factor; Semi-infinite slabs; Circular cavity

1. Introduction

Functionally graded materials (FGMs) are the new generation of composites, and important area of material science research. The physical parameters of the materials can change gradually in one direction, such as the heat conductivity, specific heat and mass density. All the properties have many potential applications, e.g., thermal barrier coating, thermal protection of the reentry capsule, etc. As an example, having a smooth transition region between a pure metal and pure ceramic would result in a new type of materials, which combines the desirable high temperature properties and thermal resistance of a ceramic with the fracture ductility of a metal [1–3].

* Corresponding author. Tel.: +86 451 86410268.
E-mail address: fangxueqian@163.com (X.-Q. Fang).

0013-7944/$ - see front matter
doi:10.1016/j.engfracmech.2007.04.029

Nomenclature

μ_0	shear modulus of materials at the position of $x = 0$
ρ_0	density of materials at the position of $x = 0$
β	non-homogeneity parameter of materials
a	radius of the circular cavity
b, c_1, c_2	the distance between the center of the cavity and the boundaries of the semi-infinite slab
τ_{xz}, τ_{yz}	anti-plane shear stress
u	displacement field in materials
c_s	wave speed of shear waves
ω	circular frequency of the incident waves
k	wave number of elastic waves
$w(x, y)$	function introduced for derivation
$z = x + iy$	complex variable in the physical plane
$\bar{z} = x - iy$	the conjugate complex value of $z = x + iy$
$H_n^{(1)}(\cdot)$	the nth Hankel function of the first kind
A_n	mode coefficients of the scattered waves
$\mathrm{Re}(z)$	the real part of complex variable z
$\mathrm{Im}(z)$	the image part of complex variable z
p	wave number in the x-direction
q	wave number in the y-direction
$u^{(i)}$	incident wave field
$u^{(s)}$	scattered wave field
u^{p}	propagating wave in functionally graded materials
u_0	displacement amplitude of the wave fields
$J_n(\cdot)$	the nth Bessel function of the first kind
$H_n^{(1)}(\cdot)$	the w_0 Hankel function of the first kind
τ_{rz}	radial shear stress
τ_0	the maximum magnitude of the stress in the incident direction
DSCF	dynamic stress concentration factor

To meet the requirements of engineering design, it is necessary to make cutouts in functionally graded material structures, and some failures such as cavities and cracks may also occur in the structures. Under dynamic loads, the stress around and near the discontinuities may increase sharply, which causes the decrease of the strength and service life of the structures. The theoretical analysis and experimental investigations of this problem have received considerable attention over past several decades [4–8].

Using the boundary element method, Rice and Sadd [4] investigated the propagation and scattering of SH waves in semi-infinite homogeneous materials containing subsurface cavities, and the numerical solution of the dynamic stress around the cavity was obtained. By making use of Laplace and Fourier integral transforms and a numerical Laplace inversion technique, Li and Weng [5] presented the dynamic stress intensity factor of a cylindrical crack located in a functionally graded material interlayer between two coaxial elastic dissimilar homogeneous cylinders and subjected to a torsional impact loading, and the effect of parameters on dynamic stress intensity factor was also analyzed. Assuming an exponential spatial variation of the elastic properties, Ueda [6] adopted the Fourier transform technique to compute the dynamic stress intensity factor of the surface crack in a layered plate with a functionally graded non-homogeneous interface, and analyzed the effect of the geometric and material parameters on the variations of dynamic stress intensity factors. Applying the method of finite element, Rousseau and Tippur [7] analyzed the effect of different elastic gradient profiles on the fracture behavior of dynamically loaded functionally graded materials having cracks parallel to the elastic gradient. Based on the integral equation for the crack in a non-homogeneous medium with a continuously differentiable shear modulus, Chan et al. [8] studied the dynamic stress of the crack under shear waves in FGMs.

Although these numerical methods are very useful tools for these problems, it is also very important to determine the physical behavior of the problems with analytical method. Pao and Chao [9] studied the elastic wave scattering and dynamic stress concentration in a thin plate with cutouts, and the analytical and numerical solutions of the problem were presented. Image method was also applied to investigate analytically the elastic wave scattering and dynamic stress concentration in the plate having a circular cavity [10] and in the semi-infinite thin plate with a cutout [11].

It is well known that many practical engineering structures have boundaries, and are not ideally infinite. However, because the boundaries of structures reflect the elastic waves and vibration, complex problems such as the multiple scattering of elastic waves may arise. Most recently, Fang et al. have studied the strain energy density around a circular cavity buried in semi-infinite functionally graded materials subjected to shear waves [12]. The main objective of this paper is to extend the work by Fang et al. [12] to the semi-infinite slab of functionally graded materials with a circular cavity. The multiple scattering and dynamic stress resulting from the circular cavity are investigated. The wave fields are expanded by employing wave functions expansion method, and the expanded mode coefficients are obtained by satisfying the boundary condition of the cavity. Image method is used to satisfy the boundary condition of traction free surfaces. The analytical solution of this problem is presented. The effects of the geometric and material parameters on the dynamic stress concentration factors around the cavity are also analyzed.

2. Wave motion equation and its solution

A semi-infinite slab of functionally graded materials is considered, which is depicted in Fig. 1. A circular cavity with radius a is buried in the slab, the distances between the center of the cavity and the boundaries of the semi-infinite slab are b, c_1 and c_2. An anti-plane shear wave is incident on the semi-infinite edge in the positive x-direction.

For mathematical convenience, the shear modulus and density of materials vary continuously in the x-direction, the variations of them are assumed by

$$\mu(x) = \mu_0 \exp(2\beta x), \quad \rho(x) = \rho_0 \exp(2\beta x), \tag{1}$$

where μ_0 and ρ_0 are the shear modulus and density of materials at the position of $x = 0$, respectively, and β is a non-homogeneity parameter which denotes the exponent of spatial variation of the shear modulus and density

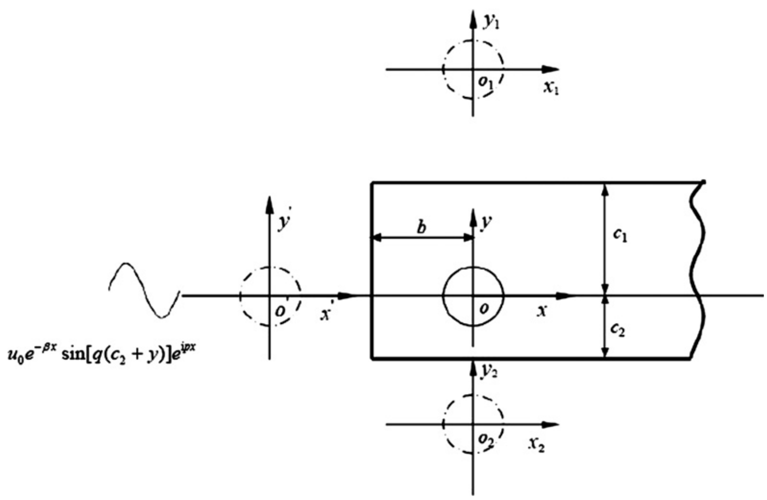

Fig. 1. A semi-infinite slab of functionally graded materials with a circular cavity.

of materials [2]. Though the variations are unrealistic, it would allow us to comprehend the effect of material gradient on the dynamic stress around the cavity and can provide references for reducing the dynamic stress.

The anti-plane governing equation in materials is described as

$$\frac{\partial \tau_{xz}}{\partial x} + \frac{\partial \tau_{yz}}{\partial y} = \rho \frac{\partial^2 u}{\partial t^2}, \tag{2}$$

where τ_{xz} and τ_{yz} are the anti-plane shear stresses, and u is the total wave field in materials.

The constitutive relations of anti-plane shear displacement are

$$\tau_{xz} = \mu(x)\frac{\partial u}{\partial x}, \quad \tau_{yz} = \mu(x)\frac{\partial u}{\partial y}. \tag{3}$$

Substitution of Eq. (3) into Eq. (2) yields the following equation

$$\frac{\partial^2 u}{\partial x^2} + \frac{\partial^2 u}{\partial y^2} + 2\beta\frac{\partial u}{\partial x} = \frac{1}{c_s^2}\frac{\partial^2 u}{\partial t^2}, \tag{4}$$

where $c_s = \sqrt{\mu_0/\rho_0}$ is the wave speed of shear waves.

The steady solution of the problem is investigated. Let $u = U\exp(-\mathrm{i}\omega t)$, Eq. (4) can be changed into the following equation

$$\nabla^2 U + 2\beta\frac{\partial U}{\partial x} + k^2 U = 0, \tag{5}$$

where ω is the circular frequency of the incident waves, and $k = \omega/c_s$ is the wave number of elastic waves.

The form of the solution of Eq. (5) can be proposed as

$$U = \exp(-\beta x)w(x,y), \tag{6}$$

where $w(x,y)$ is the function introduced for derivation.

Substituting Eq. (6) into (5), one can see that function $w(x,y)$ should satisfy the following equation

$$\nabla^2 w + \kappa^2 w = 0, \tag{7}$$

where $\kappa = (k^2 - \beta^2)^{1/2}$. It should be noted that $k^2 > \beta^2$.

According to Eqs. (5)–(7), it can be seen that there exist elastic waves with the form of $U\mathrm{e}^{-\mathrm{i}\omega t} = u_0\exp(-\beta x)\mathrm{e}^{\mathrm{i}(\kappa x - \omega t)}$, which denotes the propagating wave with its amplitude of vibration attenuating in the x-direction.

In the following, in order to concisely express the scattering fields of many image cavities, the complex variable method is applied. The complex variables $z = x + \mathrm{i}y$ and $\bar{z} = x - \mathrm{i}y$ are introduced, then Eq. (7) can be transformed into the equation about the variables of z and $\bar{z}$ [14,15]

$$\frac{\partial^2 w}{\partial z \partial \bar{z}} + \left(\frac{\kappa}{2}\right)^2 w = 0. \tag{8}$$

The general solution of the scattered field u^s resulting from the circular cavity in FGMs is expressed as [12,13]

$$u^s = \exp(-\beta r\cos\theta)\sum_{n=-\infty}^{\infty} A_n H_n^{(1)}(\kappa r)\mathrm{e}^{\mathrm{i}(n\theta - \omega t)} = \exp(-\beta\,\mathrm{Re}\,z)\sum_{n=-\infty}^{\infty} A_n H_n^{(1)}(\kappa|z|)\left(\frac{z}{|z|}\right)^n \mathrm{e}^{-\mathrm{i}\omega t}. \tag{9}$$

where $H_n^{(1)}(\cdot)$ is the nth Hankel function of the first kind and denotes the outgoing waves, A_n determined by satisfying the boundary condition of the cavity are the mode coefficients of the scattered waves, and $\mathrm{Re}(z)$ denotes the real part of complex variable z. It should be noted that all wave fields have the same time variation $\mathrm{e}^{-\mathrm{i}\omega t}$, which is omitted in all subsequent representations for notational convenience.

3. The excitation of elastic waves and the total wave field

Consider an anti-plane shear wave propagating along the positive x-direction. Based on the constructive interference theory of wave fields, the propagating wave u^{p} in the semi-infinite slab of functionally graded materials can be described as

$$u^{\mathrm{p}} = f(y)\exp(-\beta x)\exp(\mathrm{i}px). \tag{10}$$

The solution of Eq. (10) should satisfy Eq. (4), and then the following expression can be obtained

$$f(y) = A\cos(qy) + B\sin(qy), \tag{11}$$

where p and q are the longitudinal and transversal wave numbers, respectively, and $p^2 = \kappa^2 - q^2 = k^2 - \beta^2 - q^2$.

Suppose that the upper and lower boundary conditions are free of traction. Thus, function $f(y)$ should satisfy the following equation

$$f(c_1)\mu(x) = 0, \quad f(-c_2)\mu(x) = 0. \tag{12}$$

So, the transversal wave number is expressed as

$$q = \frac{n\pi}{c_1 + c_2} \quad (n = 0, 1, 2, \ldots). \tag{13}$$

Substitution of Eq. (13) into Eq. (10) yields the expression of propagating wave in functionally graded materials

$$u^{\mathrm{p}} = B\sin[q(c_2 + y)]\exp(-\beta x)\exp(\mathrm{i}px). \tag{14}$$

The reflected waves are described by employing image method. Note that the $n = 1$ mode is investigated in this paper.

By using wave function expansion method and Eq. (14), the incident wave field can be proposed as [12,13]

$$u^{(\mathrm{i})} = u_0\exp(-\beta x)\sin[q(c_2 + y)]\mathrm{e}^{\mathrm{i}p(x+b)} = u_0\sin[q(c_2 + y)]\mathrm{e}^{-\beta x + \mathrm{i}pb}\sum_{n=-\infty}^{\infty}\mathrm{i}^n J_n(pr)\mathrm{e}^{\mathrm{i}n\theta}, \tag{15}$$

where u_0 is the displacement amplitude of the incident waves, p is the wave number in the x-direction, and $J_n(\cdot)$ is the nth Bessel function.

Considering the multiple scattering at the boundaries of $x = -b$, $y = c_1$ and $y = -c_2$ $(c_1 > 0, c_2 > 0)$ and using image method [12,13], the total scattered field resulting from the circular cavity can be described, in polar coordinate system, as

$$\begin{aligned} u^{(\mathrm{s})} = \exp(-\beta r\cos\theta)\Bigg\{ &\sum_{n=-\infty}^{\infty} A_n H_n^{(1)}(\kappa r)\mathrm{e}^{\mathrm{i}n\theta} + \sum_{n=-\infty}^{\infty} A_n(-1)^n H_n^{(1)}(\kappa r')\mathrm{e}^{-\mathrm{i}n\theta'} \\ &+ \sum_{m=1}^{\infty}\left[\sum_{n=-\infty}^{\infty} A_n H_n^{(1)}(\kappa r_m)\mathrm{e}^{\mathrm{i}n\theta_m} + \sum_{n=-\infty}^{\infty} A_n(-1)^n H_n^{(1)}(\kappa r'_m)\mathrm{e}^{-\mathrm{i}n\theta'_m}\right]\Bigg\}. \end{aligned} \tag{16}$$

To express concisely the scattering fields of many image cavities, the total scattered field is expressed in the form of complex variable [14,15]

$$\begin{aligned} u^{(\mathrm{s})} = \exp[-\beta\,\mathrm{Re}(z)]\Bigg[&\sum_{n=-\infty}^{\infty} A_n H_n^{(1)}(\kappa|z|)\left(\frac{z}{|z|}\right)^n + \sum_{n=-\infty}^{\infty} A_n(-1)^n H_n^{(1)}(\kappa|z - z_0|)\left(\frac{z - z_0}{|z - z_0|}\right)^{-n} \\ &\times \sum\nolimits_{n=-\infty}^{\infty}\sum_{m=1}^{\infty}\sum_{l=1}^{4} A_n H_n^{(1)}(\kappa|z - z_{lm}|)\left(\frac{z - z_{lm}}{|z - z_{lm}|}\right)^n \\ &+ \sum_{n=-\infty}^{\infty}\sum_{m=1}^{\infty}\sum_{l=1}^{4} A_n(-1)^n H_n^{(1)}(\kappa|z - z_0 - z_{lm}|)\left(\frac{z - z_0 - z_{lm}}{|z - z_0 - z_{lm}|}\right)^{-n}\Bigg], \end{aligned} \tag{17}$$

where $z_0 = -2b$, $z_{1m} = \mathrm{i}2(mL - c_2)$, $z_{2m} = \mathrm{i}2mL$, $z_{3m} = -\mathrm{i}2[(m-1)\ \ L + c_2]$, $z_{4m} = -2\mathrm{i}mL$, $L = c_1 + c_2$, $m = 1,2,\ldots$

The total wave field in materials is taken to be a superposition of the incident waves and the scattered waves, i.e.

$$u = u^{(\mathrm{i})} + u^{(\mathrm{s})}. \tag{18}$$

4. Determination of mode coefficients and dynamic stress concentration factor

Without loss of generality, the case that the boundary condition is free of traction is investigated. The boundary condition is that the radial shear stress is equal to zero, i.e.

$$\tau_{rz}|_{r=a} = \mu(r,\theta)\left.\frac{\partial u}{\partial r}\right|_{r=a} = 0. \tag{19}$$

Substituting Eq. (18) into Eq. (19), the following equations can be obtained:

$$\sum_{n=-\infty}^{+\infty} E_n X_n = E, \tag{20}$$

where

$$\begin{aligned}
E_n = {} & -\beta \mathrm{Re}\left(\frac{z}{|z|}\right)\exp[-\beta \mathrm{Re}(z)]\left[H_n^{(1)}(\kappa|z|)\left(\frac{z}{|z|}\right)^n + (-1)^n H_n^{(1)}(\kappa|z-z_0|)\left(\frac{z-z_0}{|z-z_0|}\right)^{-n}\right] \\
& + \exp[-\beta \mathrm{Re}(z)]\Bigg\{\frac{\kappa}{2}\left[H_{n-1}^{(1)}(\kappa|z|) - H_{n+1}^{(1)}(\kappa|z|)\right]\left(\frac{z}{|z|}\right)^n + \sum_{m=1}^{\infty}\sum_{l=1}^{4} H_n^{(1)}(\kappa|z-z_{lm}|)\left(\frac{z-z_{lm}}{|z-z_{lm}|}\right)^n \\
& + \sum_{m=1}^{\infty}\sum_{l=1}^{4}(-1)^n H_n^{(1)}(\kappa|z-z_0-z_{lm}|)\left(\frac{z-z_0-z_{lm}}{|z-z_0-z_{lm}|}\right)^{-n} \\
& + \frac{1}{2}\kappa(-1)^n\frac{1}{|z|}|z-z_0|\mathrm{Re}\left(\frac{z}{z-z_0}\right)\left[H_{n-1}^{(1)}(\kappa|z-z_0|) - H_{n+1}^{(1)}(\kappa|z-z_0|)\right]\left(\frac{z-z_0}{|z-z_0|}\right)^{-n} \\
& + \mathrm{i}n(-1)^n\frac{1}{|z|}\mathrm{Im}\left(\frac{z}{z-z_0}\right)H_n^{(1)}(\kappa|z-z_0|)\left(\frac{z-z_0}{|z-z_0|}\right)^{-n} \\
& + \frac{1}{2}\sum_{m=1}^{\infty}\sum_{l=1}^{4}\kappa\frac{1}{|z|}|z-z_{lm}|\mathrm{Re}\left(\frac{z}{z-z_{lm}}\right)\left[H_{n-1}^{(1)}(\kappa|z-z_{lm}|) - H_{n+1}^{(1)}(\kappa|z-z_{lm}|)\right]\left(\frac{z-z_{lm}}{|z-z_{lm}|}\right)^n \\
& + \sum_{m=1}^{\infty}\sum_{l=1}^{4}\mathrm{i}n\frac{1}{|z|}\left(\frac{z-z_{lm}}{|z-z_{lm}|}\right)^n\mathrm{Im}\left(\frac{z}{z-z_{lm}}\right)H_n^{(1)}(\kappa|z-z_{lm}|)\left(\frac{z-z_{lm}}{|z-z_{lm}|}\right)^n \\
& + \frac{1}{2}\sum_{m=1}^{\infty}\sum_{l=1}^{4}(-1)^n\kappa\frac{1}{|z|}|z-z_0-z_{lm}|\mathrm{Re}\left(\frac{z}{z-z_0-z_{lm}}\right) \\
& \times\left[H_{n-1}^{(1)}(\kappa|z-z_0-z_{lm}|) - H_{n+1}^{(1)}(\kappa|z-z_0-z_{lm}|)\right]\left(\frac{z-z_0-z_{lm}}{|z-z_0-z_{lm}|}\right)^{-n} \\
& + \sum_{m=1}^{\infty}\sum_{l=1}^{4}(-1)^n\mathrm{i}n\frac{1}{|z|}\mathrm{Im}\left(\frac{z}{z-z_0-z_{lm}}\right)H_n^{(1)}(\kappa|z-z_0-z_{lm}|)\left(\frac{z-z_0-z_{lm}}{|z-z_0-z_{lm}|}\right)^{-n}\Bigg\},
\end{aligned} \tag{21}$$

$$\begin{aligned}
E &= -u_0\mathrm{e}^{-\beta x}\mathrm{e}^{\mathrm{i}p(x+b)}\{-\beta\cos\theta\sin[q(c_2+y)] + \{q\sin\theta\cos[q(c_2+y)] + \mathrm{i}p\cos\theta\sin[q(c_2+y)]\}\} \\
&= -u_0\mathrm{e}^{-\beta x+\mathrm{i}pb}\{-\beta\cos\theta\sin[q(c_2+y)] + \{q\sin\theta\cos[q(c_2+y)] + \mathrm{i}p\cos\theta\sin[q(c_2+y)]\}\} \\
&\quad\times\sum_{n=-\infty}^{\infty}\mathrm{i}^n J_n(pr)\mathrm{e}^{\mathrm{i}n\theta},
\end{aligned} \tag{22}$$

and $X_n = A_n$.

Multiplying by $e^{-is\theta}$ at both sides of Eq. (20), and then integrating from $-\pi$ to π, the following expressions can be obtained

$$\sum_{n=-\infty}^{+\infty} E_{ns}X_n = E_s \quad (s = 0, \pm 1, \pm 2, \ldots), \tag{23}$$

here the elements of E_{ns} and E_s are determined by the following equations

$$E_{ns} = \frac{1}{2\pi}\int_{-\pi}^{\pi} E_n e^{-is\theta}\,d\theta, \quad E_s = \frac{1}{2\pi}\int_{-\pi}^{\pi} E e^{-is\theta}\,d\theta. \tag{24}$$

Note that Eq. (23) is the infinite algebraic equation system determining mode coefficients A_n. Functions $H_n^{(1)}(\cdot)$ and $J_n(\cdot)$ are both convergent, so the solution of Eq. (23) can be obtained by truncating n and s [10,12,13].

In the following analysis, it is convenient to make the variables dimensionless. To accomplish this step, we may introduce a representative length scale a, where a is the radius of the circular cavity. The following dimensionless variables and quantities have been chosen for computation: the incident wave number is $ka = 0.01$–2.0, the distance between the center of the cavity and the semi-infinite boundary is $b/a = 1.1$–5.0, the distance between the center of the cavity and the upper boundary is $c_1/a = 3.0$–8.0, the distance between the center of the cavity and the lower boundary is $c_2/a = 3.0$–8.0, and the non-homogeneity parameter is $\beta a = -0.1$ to 0.1.

According to the definition of the dynamic stress concentration factor (DSCF), the DSCF is the ratio of the hoop shear stress around the cavity and the maximum stress [13]. Thus, the DSCF around the circular cavity in the semi-infinite slab of functionally graded materials is expressed as

$$\mathrm{DSCF} = |\tau_{\theta z}/\tau_0|, \tag{25}$$

$$\begin{aligned}
\tau_{\theta z} = \mu(r,\theta)\frac{1}{r}\frac{\partial u}{\partial\theta} = -\beta\mu(z,\bar{z})\exp[-\beta\mathrm{Re}(z)]\Bigg\{&\sum_{n=-\infty}^{\infty} A_n H_n^{(1)}(\kappa|z|)\left(\frac{z}{|z|}\right)^n \\
&+ \sum_{n=-\infty}^{\infty} A_n(-1)^n H_n^{(1)}(\kappa|z-z_0|)\left(\frac{z-z_0}{|z-z_0|}\right)^{-n} + \sum_{n=-\infty}^{\infty} A_n \sum_{m=1}^{\infty}\sum_{l=1}^{4} H_n^{(1)}(\kappa|z-z_{lm}|)\left(\frac{z-z_{lm}}{|z-z_{lm}|}\right)^n \\
&- \sum_{n=-\infty}^{\infty}\sum_{m=1}^{\infty}\sum_{l=1}^{4}(-1)^n A_n H_n^{(1)}(\kappa|z-z_0-z_{lm}|)\left(\frac{z-z_0-z_{lm}}{|z-z_0-z_{lm}|}\right)^{-n}\Bigg\} \\
&+ \frac{1}{\mathrm{Re}(z)}\exp[-\beta\mathrm{Re}(z)]\Bigg\{\frac{1}{2}\kappa\sum_{n=-\infty}^{\infty} A_n[H_{n-1}^{(1)}(\kappa|z|) - H_{n+1}^{(1)}(\kappa|z|)]\left(\frac{z}{|z|}\right)^n \\
&- \sum_{n=-\infty}^{\infty}\frac{\kappa}{2}(-1)^n A_n|z-z_0|\mathrm{Im}\left(\frac{z}{z-z_0}\right)[H_{n-1}^{(1)}(\kappa|z-z_0|) - H_{n+1}^{(1)}(\kappa|z-z_0|)]\left(\frac{z-z_0}{|z-z_0|}\right)^{-n} \\
&+ \sum_{n=-\infty}^{\infty}(-1)^n A_n in\mathrm{Re}\left(\frac{z}{z-z_0}\right)H_n^{(1)}(\kappa|z-z_0|)\left(\frac{z-z_0}{|z-z_0|}\right)^{-n} \\
&- \sum_{n=-\infty}^{\infty}\sum_{m=1}^{\infty}\sum_{l=1}^{4}\frac{\kappa}{2}A_n|z-z_{lm}|\mathrm{Im}\left(\frac{z}{z-z_{lm}}\right)\left[H_{n-1}^{(1)}(\kappa|z-z_{lm}|) - H_{n+1}^{(1)}(\kappa|z-z_{lm}|)\right]\left(\frac{z-z_{lm}}{|z-z_{lm}|}\right)^n \\
&+ \sum_{n=-\infty}^{\infty}\sum_{m=1}^{\infty}\sum_{l=1}^{4} A_n in\mathrm{Re}\left(\frac{z}{z-z_0}\right)H_n^{(1)}(\kappa|z-z_{lm}|)\left(\frac{z-z_{lm}}{|z-z_{lm}|}\right)^n \\
&- \sum_{n=-\infty}^{\infty}\sum_{m=1}^{\infty}\sum_{l=1}^{4}\frac{\kappa}{2}(-1)^n A_n|z-z_0-z_{lm}|\mathrm{Im}\left(\frac{z}{z-z_0-z_{lm}}\right) \\
&\times\left[H_{n-1}^{(1)}(\kappa|z-z_0-z_{lm}|) - H_{n+1}^{(1)}(\kappa|z-z_0-z_{lm}|)\right]\left(\frac{z-z_0-z_{lm}}{|z-z_0-z_{lm}|}\right)^n \\
&- \sum_{n=-\infty}^{\infty}\sum_{m=1}^{\infty}\sum_{l=1}^{4}(-1)^n A_n in\mathrm{Re}\left(\frac{z}{z-z_0-z_{lm}}\right)H_n^{(1)}(\kappa|z-z_0-z_{lm}|)\left(\frac{z-z_0-z_{lm}}{|z-z_0-z_{lm}|}\right)^{-n}\Bigg\} \\
&+ u_0 e^{-\beta x}\mu(r,\theta)\{(\beta - ip)\sin\theta\sin[q(c_2+y)] + q\cos\theta\cos[q(c_2+y)]\}e^{ip(x+b)},
\end{aligned} \tag{26}$$

here τ_0 is the maximum magnitude of the stress in the incident direction, and $\tau_0(r,\theta) = (\beta^2 + p^2)^{\frac{1}{2}} = (k^2 + \pi^2/L^2)^{\frac{1}{2}}$.

5. Numerical examples

Fatigue failures often occur in the regions with high stress concentration, so an understanding of the distribution of the dynamic stress around the cavity is very useful in structural design.

According to the expression of DSCF, the DSCFs around the circular cavity are computed. It is found that the truncations of n, s and m at 12 in Eqs. (23) and (26) give practically adequate results at any desired wave numbers.

Fig. 2 illustrates the angular distribution of the DSCFs around the circular cavity with parameters: $\beta = 0$, $b/a = 1.1$, $c_1/a = 8.0$, $c_2/a = 8.0$. Note that in this case the upper and lower boundaries have no effect on the DSCFs around the cavity. It can be seen that when the distance is $b/a = 1.1$, because of the multiple scattering of elastic waves between the cavity and the semi-infinite edge, the DSCFs at the positions near the semi-infinite edge are greater than that at the symmetrical positions about the y axis. The DSCFs around the cavity increase with increasing incident wave number. When the incident wave number is relatively great, the edge of the semi-infinite structure has greater effect on the distribution of the DSCFs around the cavity.

Fig. 3 illustrates the angular distribution of the DSCFs around the circular cavity with parameters: $\beta = 0$, $b/a = 5.0$, $c_1/a = 8.0$, $c_2/a = 8.0$. It can be seen that the maximum dynamic stress decreases with the increase of

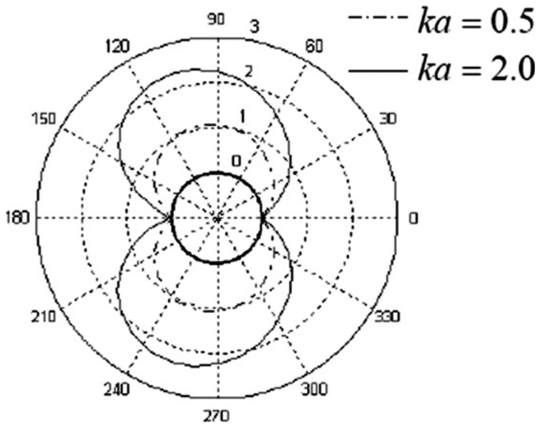

Fig. 2. Angular distribution of dynamic stress around the cavity ($\beta = 0$, $b/a = 1.1$, $c_1/a = 8.0$, $c_2/a = 8.0$).

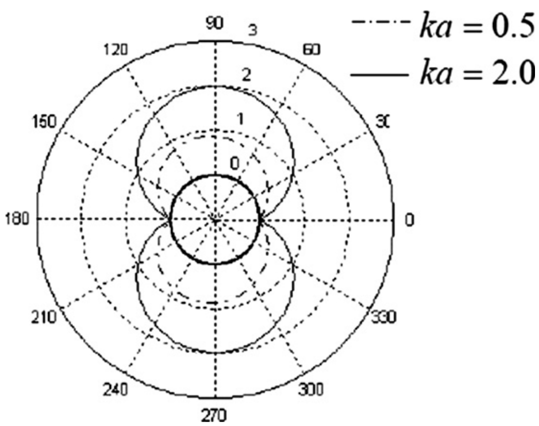

Fig. 3. Angular distribution of dynamic stress around the cavity ($\beta = 0$, $b/a = 5.0$, $c_1/a = 8.0$, $c_2/a = 8.0$).

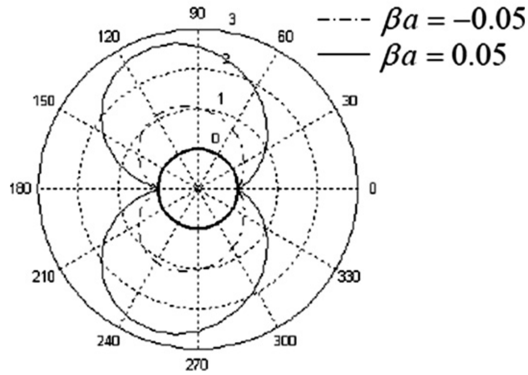

Fig. 4. Angular distribution of dynamic stress around the cavity ($ka = 2.0$, $b/a = 1.1$, $c_1/a = 8.0$, $c_2/a = 8.0$).

the value of b/a, and the angular distributions of DSCFs are approximatively symmetric about both axes. The above results show good agreement with those in literature [3].

Fig. 4 illustrates the angular distribution of the DSCFs around the circular cavity with parameters: $ka = 0.1$, $b/a = 1.1$, $c_1/a = 8.0$, $c_2/a = 8.0$. It can be seen that the DSCFs around the cavity increase with increasing non-homogeneity parameter of materials. As the non-homogeneity parameter increases, the effect

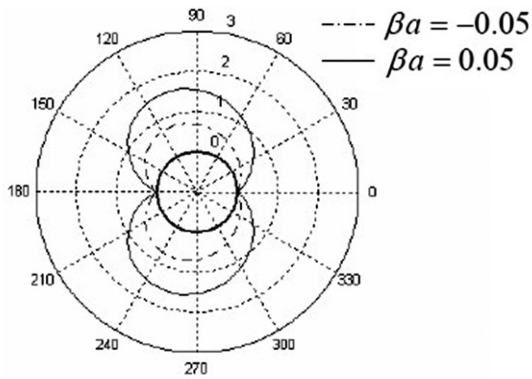

Fig. 5. Angular distribution of dynamic stress around the cavity ($ka = 2.0$, $b/a = 5.0$, $c_1/a = 8.0$, $c_2/a = 8.0$).

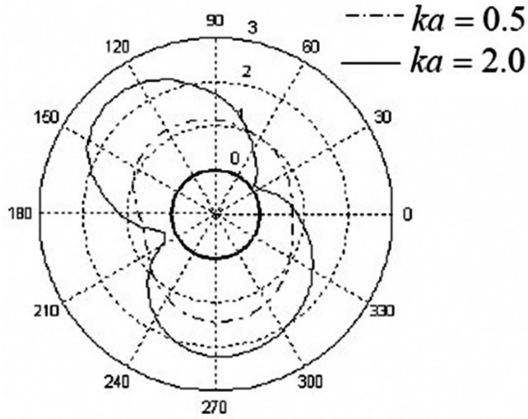

Fig. 6. Angular distribution of dynamic stress around the cavity ($\beta a = 0.05$, $b/a = 1.1$, $c_1/a = 3.0$, $c_2/a = 8.0$).

of the edge of semi-infinite materials increases. The edge makes the position of the maximum dynamic stress having a trend of shifting towards the illuminated side of the cavity. The trend of shifting is more evident when the non-homogeneity parameter is greater.

Fig. 5 illustrates the angular distribution of the DSCFs around the circular cavity with parameters: $ka = 0.1$, $b/a = 5.0$, $c_1/a = 8.0$, $c_2/a = 8.0$. One can see that when the distance ratio of b/a is great, the effect of non-homogeneity parameter on the distribution of DSCF decreases.

Fig. 6 illustrates the angular distribution of the DSCFs around the circular cavity with parameters: $\beta a = 0.05$, $b/a = 1.1$, $c_1/a = 3.0$, $c_2/a = 8.0$. It can be seen that due to the effect of the upper boundary, the maximum dynamic stress has a trend of shifting towards the illuminated side of the cavity, and the greater the incident wave number, the greater the effect of the upper boundary on the DSCF distribution around the cavity. In this case, the dynamic stresses at the position of $\theta = 0$ and π are greater than those in Figs. 2 and 4.

Fig. 7 displays the angular distribution of the DSCFs around the circular cavity with parameters: $\beta a = 0.05$, $b/a = 5.0$, $c_1/a = 3.0$, $c_2/a = 8.0$. It can be seen that the dynamic stress at the position of $\theta = 0$ and π becomes great. Comparing the results with those in Fig. 6, one can see that as the distance ratio of b/a increases, the distribution of the dynamic stress around the cavity is about symmetry about the y axis. However, the dynamic stresses near the upper boundary are less than that near the lower boundary.

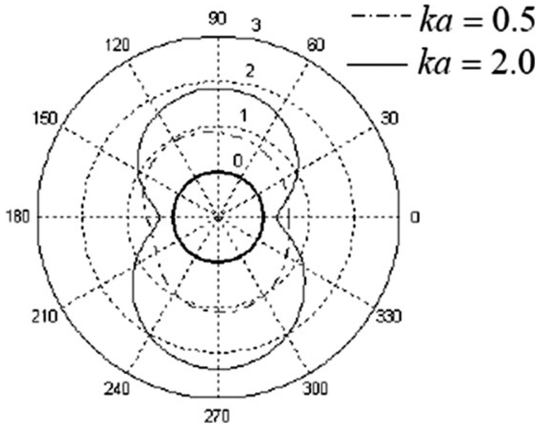

Fig. 7. Angular distribution of dynamic stress around the cavity ($\beta a = 0.05$, $b/a = 5.0$, $c_1/a = 3.0$, $c_2/a = 8.0$).

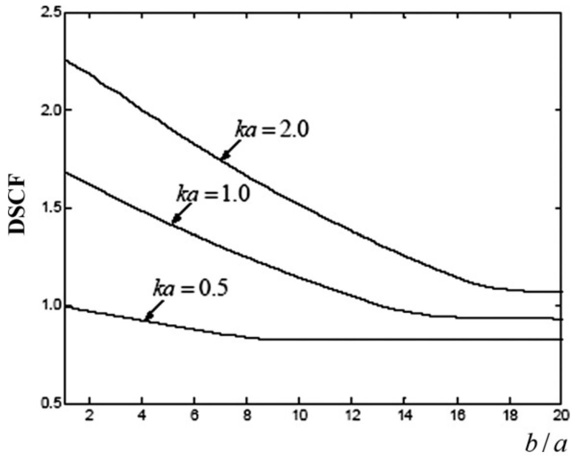

Fig. 8. Dynamic stress concentration factor as a function of b/a ($\beta = 0$, $\theta = \pi/2$, $c_1/a = 8.0$, $c_2/a = 8.0$).

Fig. 8 shows the dynamic stress at the position of $\theta = \pi/2$ as a function of the distance ratio b/a with parameters: $\beta = 0$, $c_1/a = 8.0$, $c_2/a = 8.0$. The dynamic stress at $\theta = \pi/2$ decreases as the value of b/a increases. When the value of b/a is greater than a certain number, the dynamic stresses tend to be invariable, and the number increases as the wave number increases. It is clear that the dynamic stress increases with increasing wave number. When the value of b/a is small, the variation of dynamic stress with incident wave number is great. However, if the value of b/a is great, the variation is small. It is also clear that if the wave number is small, the variation of dynamic stress with the value of b/a is small.

Fig. 9 shows the dynamic stress at the position of $\theta = \pi/2$ as a function of the distance ratio b/a with parameters: $\beta a = 0.05$, $c_1/a = 8.0$, $c_2/a = 8.0$. From Figs. 8 and 9, one can see that when the value of b/a is small, the dynamic stress at the position of $\theta = \pi/2$ increases with increasing non-homogeneity parameter of FGMs. However, when the value of b/a is great, the variation of the dynamic stress with non-homogeneity parameter is small.

Fig. 10 presents the dynamic stress at the position of $\theta = \pi/2$ as a function of the distance ratio b/a with parameters: $\beta a = 0.05$, $c_1/a = 3.0$, $c_2/a = 8.0$. It can be seen that the DSCFs first decrease with the distance ratio b/a, and then tend to be invariable as b/a further increase. Comparing the results with those in Fig. 9, it is found that because the maximum dynamic stress has a trend of shifting towards the illuminated

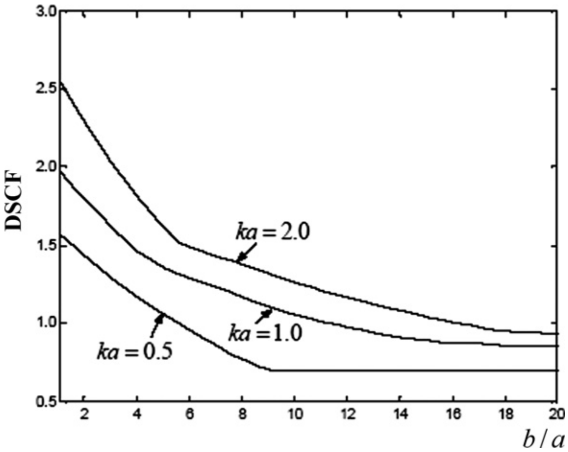

Fig. 9. Dynamic stress concentration factor as a function of b/a ($\beta a = 0.05$, $\theta = \pi/2$, $c_1/a = 8.0$, $c_2/a = 8.0$).

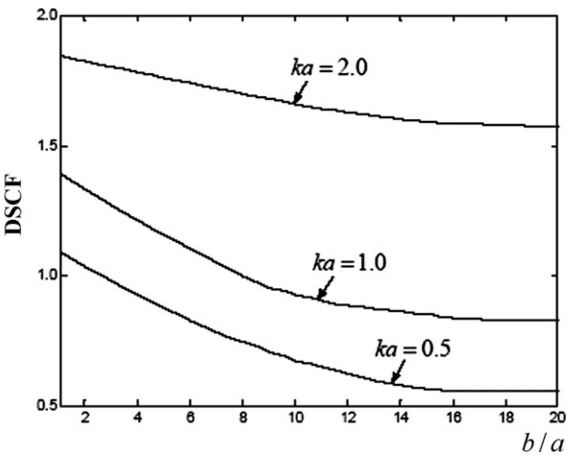

Fig. 10. Dynamic stress concentration factor as a function of b/a ($\beta a = 0.05$, $\theta = \pi/2$, $c_1/a = 3.0$, $c_2/a = 8.0$).

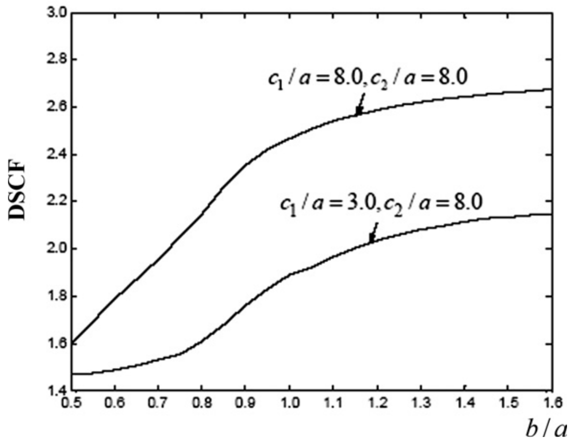

Fig. 11. Dynamic stress concentration factor as a function of ka ($\beta a = 0.1$, $\theta = \pi/2$, $b/a = 1.1$).

side of the cavity, the dynamic stress at $\theta = \pi/2$ becomes small. It is also clear that the variation of dynamic stress with the value of b/a decreases as the value of c_1/a decreases.

Fig. 11 shows the dynamic stress at the position of $\theta = \pi/2$ as a function of dimensionless wave number ka with parameters: $\beta a = 0.1$, $b/a = 1.1$. It can be seen that the DSCFs increase as the dimensionless wave number increases, and then tend to be invariable as ka further increases. Because of the effect of the upper and lower boundaries, the maximum dynamic stress deviates from the position of $\theta = \pi/2$. So when the distance between the center of the cavity and the upper boundary decreases, the dynamic stress at this position decreases. In the region of low frequency, if the distance between the center of the cavity and the upper boundary is small, the variation of the dynamic stress with dimensionless wave number is small. However, when the distance between the center of the cavity and the upper boundary is great, the variation of the dynamic stress with dimensionless wave number is great in the region of low frequency.

6. Discussion

Through examples, one can see that for the semi-infinite homogeneous materials, our results are in good agreements with the solutions in previous literatures. The non-homogeneity parameter of materials has great effect on the values and distribution of the dynamic stress concentration factors around the cavity when the distance ratios of b/a, c_1/a and c_2/a are small. The dynamic stress around the circular cavity increases with increasing non-homogeneity parameter and incident wave number. When the values of b/a and c_1/a are small, the distribution of the maximum dynamic stress varies greatly, and deviates from the position of $\theta = \pi/2$. The effects of the distance ratios of b/a, c_1/a and c_2/a on the angular distribution of the DSCFs around the cavity also increase with increasing dimensionless wave number. The maximum dynamic stress around the cavity increases greatly with an increase of the frequency of dynamic load when the values of b/a and c_1/a are small and the frequency of dynamic load is relatively high.

7. Conclusions

The elastodynamic problem of a circular cavity in a semi-infinite slab of functionally graded materials under anti-plane shear waves is analyzed by employing image method and wave functions expansion method. The case that the cavity is free of traction is investigated. The analytical solution and numerical solution of the dynamic stress concentration factors around the cavity are presented and analyzed.

It can be concluded from this paper that to reduce the dynamic stress and avoid fatigue failures in semi-infinite exponentially graded materials, it is proposed that the non-homogeneity parameter should be less than zero in the x-direction in Fig. 1, namely, the shear modulus and density of semi-infinite functionally graded materials decrease in the x-direction. The smaller the value of b/a, the smaller the non-homogeneity parameter should be. When the values of c_1/a or c_2/a are smaller, the corresponding value of b/a should be greater. We should also choose greater values of b/a, c_1/a and c_2/a when designing the semi-infinite functionally graded materials under higher frequency load.

The analytical solutions presented in this paper may be useful for the dynamical analysis and strength design for the structure of FGMs and the analysis of fracture problems in FGMs.

Acknowledgements

The paper is supported by the National Natural Science Foundation of China (Foundation No. 10572045) and the Outstanding Youth Foundation of Hei Longjiang Province of China (Foundation No. JC-9). The authors are grateful to the anonymous reviewers for their constructive comments and suggestions.

References

[1] Gray LJ, Kaplan T, Richardson JD. Green's functions and boundary integral analysis for exponentially graded materials: heat conduction. ASME J Appl Mech 2003;70:543–9.
[2] Sutradhar A, Paulino GH, Gray LJ. Transient heat conduction in homogeneous and non-homogeneous materials by the Laplace transform Galerkin boundary element method. Engng Anal Bound Elem 2002;26:119–32.
[3] Kuo HY, Chen T. Steady and transient Green's functions for anisotropic conduction in an exponentially graded solid. Int J Solids Struct 2005;42:1111–28.
[4] Rice JM, Sadd MH. Propagation and scattering of SH-waves in semi-infinite domains using a time-dependent boundary element method. ASME J Appl Mech 1984;51:641–5.
[5] Li C, Weng GJ. Dynamic stress intensity factor of a cylindrical interface crack with a functionally graded interlayer. Mech Mater 2000;33:325–33.
[6] Ueda S. The surface crack problem for a layered plate with a functionally graded nonhomogeneous interface. Int J Fracture 2001;110:189–204.
[7] Roussseau CE, Tippur HV. Influence of elastic gradient profiles on dynamically loaded functionally graded materials: cracks along the gradient. Int J Solids Struct 2001;38:7839–56.
[8] Chan YS, Paulino GH, Fanjiang AC. The crack problem for nonhomogeneous materials under anti-plane shear loading – a displacement based formulation. Int J Solids Struct 2001;38:2989–3005.
[9] Pao YH, Chao CC. Diffractions of flexural waves by a cavity in an elastic plate. AIAA J 1964;2(11):2004–10.
[10] Hayir A, Bakirtas I. A note on plate having a circular cavity excited by plane harmonic SH waves. J Sound Vib 2004;271:241–55.
[11] Hu C, Fang XQ, Huang WH. Multiple scattering of flexural waves in a semi-infinite thin plate with a cutout. Int J Solids Struct 2007;44:436–46.
[12] Fang XQ, Hu C, Du SY. Strain energy density of a circular cavity buried in semi-infinite functionally graded materials subjected to shear waves. Theor Appl Fract Mech 2006;46:166–74.
[13] Pao YH, Mow CC. Diffraction of elastic waves and dynamic stress concentrations. New York: Crane and Russak; 1973.
[14] Shi SX. Scattering of SH-wave by the structure surface with multiple semi-cylindrical medium inclusion. Acta Aeronaut Astronaut Sin 2001;22:19–23 [in Chinese].
[15] Hashimoto M, Ujisawa K. Field description with spatial complex variables and its application to scattering and waveguide problems. IEEE T Microw Theory 1971;19:458–74.